JOURNAL OF SOLID STATE CHEMISTRY **131,** 108–114 (1997)
ARTICLE NO. SC977355

Relationship between Crystal Structure and Electrical Properties of $Nd(Cr_{1-x}Fe_x)O_3$

Hideki Taguchi

Research Laboratory for Surface Science, Faculty of Science, Okayama University, Okayama 700, Japan

Received July 26, 1996; in revised form December 24, 1996; accepted February 18, 1997

Perovskite-type $Nd(Cr_{1-x}Fe_x)O_3$ was synthesized in the range $0.0 \leq x \leq 1.0$, and has the orthorhombic $GdFeO_3$-type structure with space group *Pnma*. The increase of the (Cr, Fe)–O distance and the effective magnetic moment (μ_{eff}) indicates that the Fe^{3+} ion is in the high-spin state with the $(d\varepsilon)^3(d\gamma)^2$ electronic configuration. Rietveld analysis indicates that the increase of the (Cr, Fe)–O distance and the decrease of the angles for (Cr, Fe)–O(1 and 2)–(Cr, Fe) make π-bonding decrease. From the electrical resistivity (ρ) measurement, $Nd(Cr_{1-x}Fe_x)O_3$ is a semiconductor with activation energy (E_a) $\approx 0.16-\approx 0.89$ eV. The temperature independence of the Seebeck coefficient (α) indicates that the mobility (μ) decreases with increasing x. © 1997 Academic Press

INTRODUCTION

$NdCrO_3$ has an orthorhombic perovskite-type structure with $a = 0.5430$ nm, $b = 0.7692$ nm, and $c = 0.5488$ nm, and exhibits antiferromagnetism with a Néel temperature (T_N) of 224 K (1, 2). The magnetic susceptibility indicates that the electronic configuration of a Cr^{3+} ion is $(d\varepsilon)^3(d\gamma)^0$. $NdCrO_3$ exhibits *p*-type semiconducting behavior above room temperature (2). The activation energy (E_a) calculated from the linear portion of the log ρ–$1000/T$ curve is ≈ 0.28 eV (3). Rao *et al.* reported that orthorhombic perovskite-type $LaCrO_3$ is a *p*-type semiconductor, and three 3*d* electrons of the Cr^{3+} ion are all localized and the Fermi level lies between the t_{2g}^* level and narrow e_g^* levels (4). Since the ionic radius and the electronegativity of a La^{3+} ion are nearly equal to those of a Nd^{3+} ion, the band structure of $NdCrO_3$ is considered to resemble the band structure of $LaCrO_3$ (5, 6).

Taguchi (7, 8) investigated the relationship between the crystal structure and the electrical properties of $Nd(Cr_{1-x}Mn_x)O_3$ and $Nd(Cr_{1-x}Co_x)O_3$. $Nd(Cr_{1-x}Mn_x)O_3$ is the *p*-type semiconductor and has maximum activation energy (E_a) at $x = 0.2$. The (Cr, Mn)–O distance and the effective magnetic moment (μ_{eff}) indicate that the spin state of the Mn^{3+} ion is high. $Nd(Cr_{1-x}Co_x)O_3$ is the *p*-type semiconductor with $E_a = \approx 0.18-\approx 0.24$ eV. The decrease of the (Cr, Co)-O distance and the effective magnetic moment (μ_{eff}) indicates that the Co^{3+} ion is in the low-spin state with the $(d\varepsilon)^6(d\gamma)^0$ at low temperature. The $1/\chi$–T curve exhibits a plateau with increasing temperature, and this plateau indicates the temperature interval where there is a conversion from the low-spin state of the Co^{3+} ion to a mixed spin state.

$NdFeO_3$ also has the orthorhombic perovskite-type structure with $a = 0.5450$ nm, $b = 0.7761$ nm, and $c = 0.5587$ nm (9), and exhibits weak ferromagnetism with a Curie temperature (T_c) of 693 K (10). Koehler *et al.* performed the neutron diffraction measurement of $NdFeO_3$ to investigate the magnetic properties (9). The magnitude of the ordered iron moment at temperature saturation is 4.57 Bohr magneton in $NdFeO_3$. Eibschütz *et al.* performed differential thermal analysis (DTA) and measured Mössbauer spectra of $LnFeO_3$ (Ln = La–Lu) (10). The quadrupole splitting, isomer shift, Curie temperature, and internal field vary greatly.

The electrical conductivity of $NdCrO_3$ is considered to be produced by the thermal excitation of the 3*d* electrons from the localized t_{2g}^* level to the narrow e_g^* orbital. If there are more than three 3*d* electrons and the excess 3*d* electrons exist in the narrow e_g^* orbital, it is assumed that the electrical conductivity may increase with increasing x. Magnetic measurement indicates that the Fe^{3+} ion in $NdFeO_3$ has five 3*d* electrons (9). In the present study, $Nd(Cr_{1-x}Fe_x)O_3$ ($0.0 \leq x \leq 1.0$) was synthesized to refine its structure, and the electrical resistivity, Seebeck coefficient, and magnetic properties were measured. These results will provide information regarding the cation–anion–cation overlap in perovskite-type $Nd(Cr_{1-x}Fe_x)O_3$.

EXPERIMENTAL

$Nd(Cr_{1-x}Fe_x)O_3$ ($0.0 \leq x \leq 1.0$) was prepared by a standard ceramic technique. Dried Nd_2O_3, Cr_2O_3, and Fe_2O_3 powders were weighed in appropriate proportions and milled for a few hours with acetone. After the mixed powders were dried at 373 K, they were calcined at 1173 K for a few

0022-4596/97 $25.00
Copyright © 1997 by Academic Press
All rights of reproduction in any form reserved.

hours in air and then fired at 1573 K for 24 h in a flow of pure oxygen gas. In order to measure the electrical properties, the powders were pressed into a pellet form under a pressure of 50 MPa, and the pellet was sintered at 1573 K for 12 h in a flow of pure oxygen gas.

The phases of the samples were identified by X-ray powder diffraction (XRD) with monochromatic Cu$K\alpha$ radiation. The cell constants of the samples were determined from high-angle reflections with Si as an external standard. The structure refinement was carried out by Rietveld analysis of the XRD data with the RIETAN program written by Izumi (11). XRD data were collected by step scanning over the angular range $20^\circ \leq 2\theta \leq 100^\circ$ in increments of 0.02° (2θ) with monochromatic Cu$K\alpha$ radiation.

The electrical resistivity (ρ) of the samples was measured by a standard four-electrode technique in the temperature range $300 \leq T \leq 1000$ K. The Seebeck coefficient (α) was measured in the temperature range $400 \leq T \leq 1000$ K, with a heating rate of 2 K/min. The magnetic susceptibility (χ) was measured with a magnetic torsion balance in the temperature range $300\text{ K} \leq T \leq 773$ K. Differential thermal analysis (DTA) and thermal gravity (TG) were performed in the temperature range $300 \leq T \leq 873$ K.

RESULTS AND DISCUSSION

XRD patterns of $Nd(Cr_{1-x}Fe_x)O_3$ ($0.0 \leq x \leq 1.0$) were completely indexed as the orthorhombic perovskite-type structure. The relationship between the cell constants (*a*, *b*, and *c* axes) and the composition is shown in Fig. 1. The cell constants increase linearly with increasing *x*. The observed cell constants of $NdFeO_3$ ($x = 1.0$) agree with the cell constant reported by Koehler *et al.* (9). The ionic radii of a Cr^{3+} ion, an Fe^{3+} ion (low-spin state), and the Fe^{3+} ion (high-spin state) with a coordination number (CN) of 6 are 0.0615, 0.0550, and 0.0645 nm, respectively (12). The increase of the cell constants is explained by the difference in ionic radius between the Cr^{3+} and Fe^{3+} ions. The Fe^{3+} ions must be in the high-spin state with the $(d\varepsilon)^3(d\gamma)^2$ electronic configuration.

The structure refinement of $Nd(Cr_{1-x}Fe_x)O_3$ ($0.0 \leq x \leq 1.0$) was carried out by Rietveld analysis of XRD data. Both $Nd(Cr_{1-x}Mn_x)O_3$ and $Nd(Cr_{1-x}Co_x)O_3$ have the orthorhombic $GdFeO_3$-type structure with space group *Pnma* (7, 8). In the present study, it can be concluded that $Nd(Cr_{1-x}Fe_x)O_3$ has the same structure with space group *Pnma* (13). Isotropic thermal parameters (B) for Nd, Cr, Fe, O(1), and O(2) ions were fixed at 0.003 nm^2 for all samples. Refined structural parameters and residuals, R_{WP}, R_I, and R_F, are listed in Table 1 (R_{WP}, R_I, and R_F are the weighted pattern, the integrated intensity, and the structure factor, respectively). The final R_F of all samples is less than 1.63%, and the low R_F suggests that the structural model for $Nd(Cr_{1-x}Fe_x)O_3$ is reasonable.

In an orthorhombic $GdFeO_3$-type structure, A-site cations (Nd ions) coordinate with twelve anions: four O(1) and eight O(2) ions. B-site cations (Cr and Fe ions) coordinate with six anions: two O(1) and four O(2) ions. Table 2 shows the (Cr, Fe)–O distance of $Nd(Cr_{1-x}Fe_x)O_3$ calculated from the refined structural parameters. The (Cr, Fe)–O(1 and 2) distances increase with *x*. The angles for O(1)–(Cr, Fe)–O(1), O(1)–(Cr, Fe)–O(2), and O(2)–(Cr, Fe)–O(2) are 180°, 90°, and 90° or 180°, respectively. Table 3 shows the angle for (Cr, Fe)–O(1 and 2)–(Cr, Fe) calculated from the refined structure. The angles for (Cr, Fe)–O(1 and 2)–(Cr, Fe) are less than 180° and decrease with increasing *x*.

Figure 2 shows the relationship between the inverse magnetic susceptibility ($1/\chi$) of $Nd(Cr_{1-x}Fe_x)O_3$ ($0.0 \leq x \leq 1.0$)

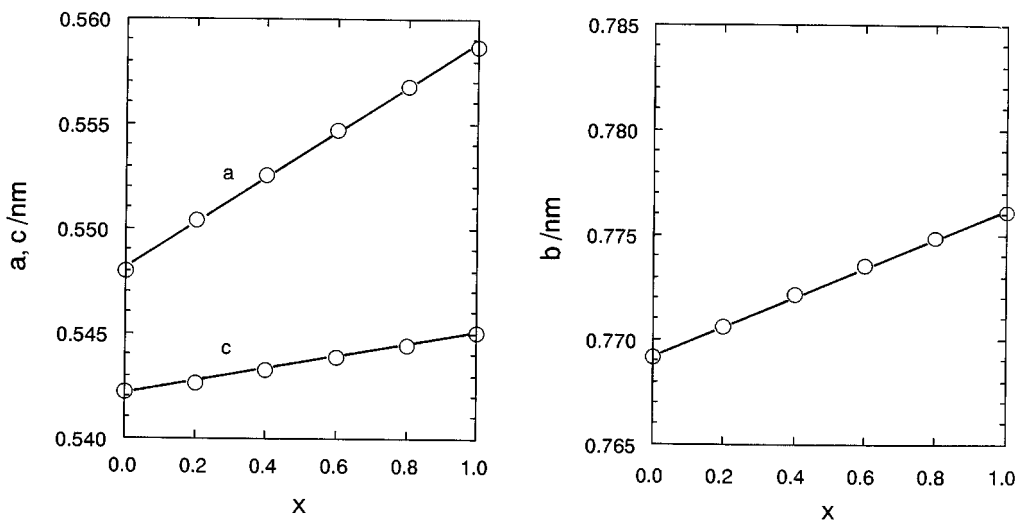

FIG. 1. Cell constants vs composition (*x*) for the system $Nd(Cr_{1-x}Fe_x)O_3$.

TABLE 1
Refined Structure Parameters for $Nd(Cr_{1-x}Fe_x)O_3$

$x = 0.0$	$a = 0.54798(1)$ nm	$b = 0.76918(2)$ nm	$c = 0.54221(1)$ nm		
	$R_{WP} = 12.69\%$	$R_I = 2.01\%$	$R_F = 1.29\%$		
Atom	Position	x	y	z	B
Nd	4(c)	0.041(1)	0.25	− 0.008(1)	0.003
Cr	4(b)	0	0	0.5	0.003
O(1)	4(c)	0.484(4)	0.25	0.082(6)	0.003
O(2)	8(d)	0.292(4)	0.041(3)	− 0.289(4)	0.003
$x = 0.2$	$a = 0.55039(1)$ nm	$b = 0.77065(2)$ nm	$c = 0.54264(1)$ nm		
	$R_{WP} = 11.63\%$	$R_I = 1.52\%$	$R_F = 0.95\%$		
Atom	Position	x	y	z	B
Nd	4(c)	0.043(1)	0.25	− 0.008(1)	0.003
Cr, Fe	4(b)	0	0	0.5	0.003
O(1)	4(c)	0.483(4)	0.25	0.090(5)	0.003
O(2)	8(d)	0.293(3)	0.040(3)	− 0.291(3)	0.003
$x = 0.4$	$a = 0.55257(1)$ nm	$b = 0.77216(2)$ nm	$c = 0.54329(1)$ nm		
	$R_{WP} = 12.34\%$	$R_I = 2.35\%$	$R_F = 1.63\%$		
Atom	Position	x	y	z	B
Nd	4(c)	0.045(1)	0.25	− 0.009(1)	0.003
Cr, Fe	4(b)	0	0	0.5	0.003
O(1)	4(c)	0.481(4)	0.25	0.089(5)	0.003
O(2)	8(d)	0.292(3)	0.040(3)	− 0.292(3)	0.003
$x = 0.6$	$a = 0.55475(1)$ nm	$b = 0.77357(1)$ nm	$c = 0.54390(1)$ nm		
	$R_{WP} = 11.46\%$	$R_I = 1.54\%$	$R_F = 1.10\%$		
Atom	Position	x	y	z	B
Nd	4(c)	0.047(1)	0.25	− 0.010(1)	0.003
Cr, Fe	4(b)	0	0	0.5	0.003
O(1)	4(c)	0.479(4)	0.25	0.092(5)	0.003
O(2)	8(d)	0.294(3)	0.041(3)	− 0.294(3)	0.003
$x = 0.8$	$a = 0.55682(1)$ nm	$b = 0.77488(1)$ nm	$c = 0.54450(1)$ nm		
	$R_{WP} = 11.29\%$	$R_I = 1.85\%$	$R_F = 1.32\%$		
Atom	Position	x	y	z	B
Nd	4(c)	0.048(1)	0.25	− 0.010(1)	0.003
Cr, Fe	4(b)	0	0	0.5	0.003
O(1)	4(c)	0.476(4)	0.25	0.093(4)	0.003
O(2)	8(d)	0.294(3)	0.041(2)	− 0.295(3)	0.003
$x = 1.0$	$a = 0.55870(1)$ nm	$b = 0.77610(1)$ nm	$c = 0.54505(1)$ nm		
	$R_{WP} = 12.90\%$	$R_I = 2.21\%$	$R_F = 1.63\%$		
Atom	Position	x	y	z	B
Nd	4(c)	0.049(1)	0.25	− 0.011(1)	0.003
Fe	4(b)	0	0	0.5	0.003
O(1)	4(c)	0.474(5)	0.25	0.093(5)	0.003
O(2)	8(d)	0.288(4)	0.049(3)	− 0.290(4)	0.003

and temperature. $Nd(Cr_{1-x}Fe_x)O_3$ ($0.0 \le x \le 0.6$) is paramagnetic in the temperature range $300\ K \le T \le 773\ K$, while $Nd(Cr_{1-x}Fe_x)O_3$ ($0.8 \le x \le 1.0$) shows unusual behavior of the $1/\chi$–T curves at ≈ 516 K for $x = 0.8$ and ≈ 676 K for $x = 1.0$, respectively. The XRD pattern of the sample ($x = 1.0$) after the magnetic measurement was completely indexed as orthorhombic $NdFeO_3$. Although each peak became broad, no extra peak was detected at all. When a bar magnet was brought near the sample ($x = 1.0$) after the magnetic measurement, the sample was attracted to the bar magnet. This fact indicates that a very small quantity of iron oxides (Fe_2O_3 or Fe_3O_4) exists in the sample. The magnetic measurement was performed at pressure of ≈ 1 Pa; therefore, a very small amount of iron oxide (Fe_2O_3 or Fe_3O_4) was produced by the decomposition of the samples under low oxygen pressure. The unusual behavior in the $1/\chi$–T curves of $x = 0.8$ and 1.0 is due to the appearance of iron oxides in the samples. The $1/\chi$–T curves obey the Curie–Weiss law at 300–500 K ($x = 0.0$), 300–520 K ($x = 0.2$), 300–570 K ($x = 0.4$), and 300–700 K ($x = 0.6$), respectively. The deviation of the $1/\chi$–T curves from the Curie–Weiss law is observed above ≈ 500 K ($x = 0.0$), 520 K ($x = 0.2$), and 570 K ($x = 0.4$). These temperatures are defined as T_M, and are shown as the arrows in Fig. 2. The effective magnetic moment (μ_{eff}) was calculated from the region obeyed the Curie–Weiss law. Figure 3 shows the relationship between μ_{eff} of $Nd(Cr_{1-x}Fe_x)O_3$ and the composition. The theoretical μ_{eff} is calculated using the equation

$$\mu_{eff} = \sqrt{(1-x)\mu^2_{Cr^{3+}} + x\mu^2_{Fe^{3+}} + \mu^2_{Nd^{3+}}}, \qquad (1)$$

where $\mu_{Cr^{3+}}$, $\mu_{Fe^{3+}}$, and $\mu_{Nd^{3+}}$ are the effective magnetic moments of the Cr^{3+} ion, the Fe^{3+} ion, and the Nd^{3+} ion,

TABLE 2
(Cr, Fe)–O Distance of $Nd(Cr_{1-x}Fe_x)O_3$

x	(Cr, Fe)–O(1) × 2 (nm)	(Cr, Fe)–O(2) × 2 (nm)	(Cr, Fe)–O(2) × 2 (nm)
0.0	0.1976(7)	0.1961(21)	0.1993(21)
0.2	0.1990(7)	0.1972(18)	0.1994(18)
0.4	0.1993(7)	0.1982(19)	0.1995(19)
0.6	0.2001(6)	0.1991(17)	0.2003(17)
0.8	0.2007(6)	0.1997(16)	0.2008(16)
1.0	0.2010(8)	0.2009(21)	0.2013(21)

TABLE 3
(Cr, Fe)–O–(Cr, Fe) Angle (°) for $Nd(Cr_{1-x}Fe_x)O_3$

x	(Cr, Fe)–O(1)–(Cr, Fe)	(Cr, Fe)–O(2)–(Cr, Fe)
0.0	153.4(18)	154.2(11)
0.2	151.0(15)	154.0(9)
0.4	151.1(15)	154.0(10)
0.6	150.2(13)	153.1(9)
0.8	149.6(12)	152.9(8)
1.0	149.7(16)	152.0(10)

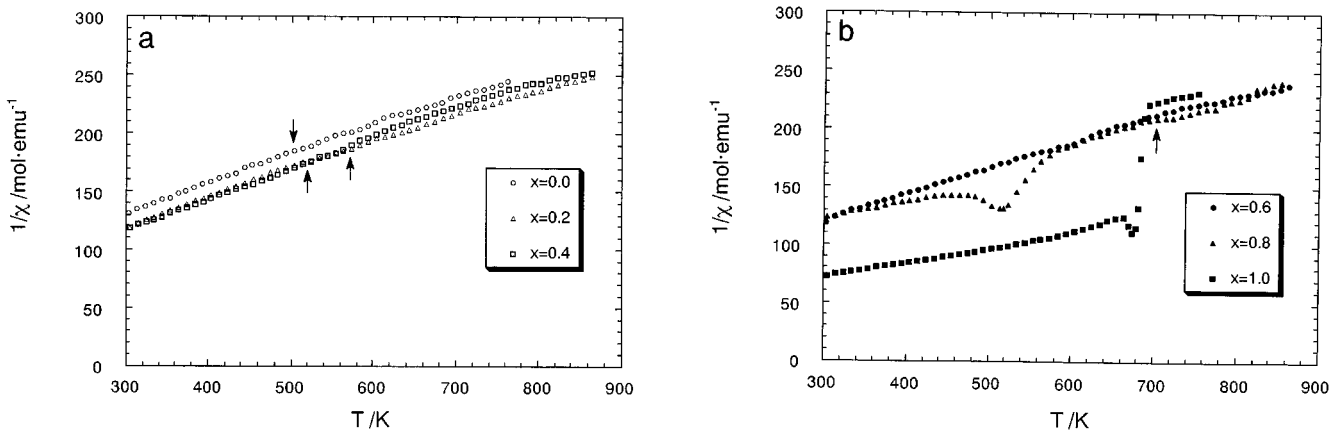

FIG. 2. Inverse magnetic susceptibility ($1/\chi$) vs temperature (T) for the system $Nd(Cr_{1-x}Fe_x)O_3$. Arrow indicates the temperature (T_M) that the $1/\chi$–T curve deviates from the Curie–Weiss law.

respectively (7, 8). From the values of the spectroscopic splitting factor (g) and total angular momentum (J) of the Nd^{3+} ion, $\mu_{Nd^{3+}}$ is calculated to be 3.62 (14). In Fig. 3, the broken lines [1] and [2] indicate the theoretical values calculated in cases of both the high-spin and low-spin states of the Fe^{3+} ion; the line [1] is the high-spin state with the $(d\varepsilon)^3(d\gamma)^2$ configuration and the line [2] is the low-spin state with the $(d\varepsilon)^5(d\gamma)^0$ configuration. According to Koehler *et al.*, the Fe^{3+} ion in $NdFeO_3$ ($x = 1.0$) is 4.75 μ_B and this value indicates that the Fe^{3+} ion is the high-spin state (9). From these results, it is obvious that the spin state of the Fe^{3+} ion in $Nd(Cr_{1-x}Fe_x)O_3$ ($0.0 \leq x \leq 1.0$) is high at room temperature.

Figure 4 shows the relationship between the logarithm of the electrical resistivity (log ρ) of $Nd(Cr_{1-x}Fe_x)O_3$ and the reciprocal temperature ($1000/T$). The decrease of log ρ with increasing temperature indicates that $Nd(Cr_{1-x}Fe_x)O_3$ is a semiconductor. The log ρ–$1000/T$ curves are linear and have deflections at $\approx$570 K ($x = 0$), 600 K ($x = 0.2$), and 640 K ($x = 0.4$). These temperatures are defined as T_R, and

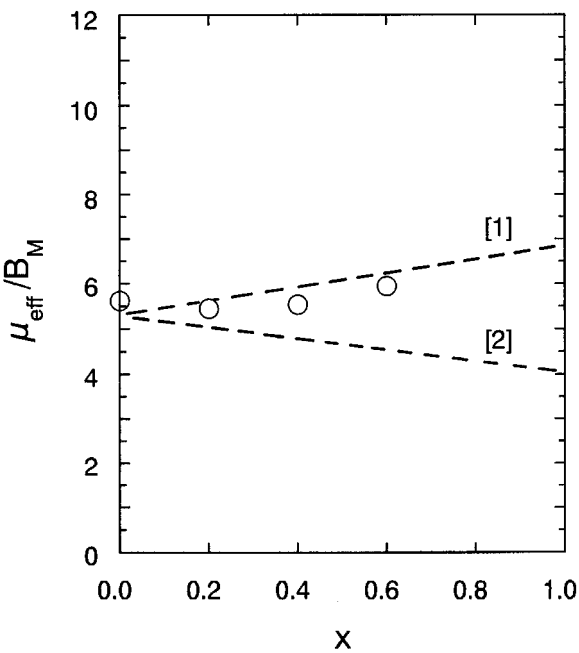

FIG. 3. Effective magnetic moment (μ_{eff}) vs composition (x) for the system $Nd(Cr_{1-x}Fe_x)O_3$. The broken lines [1] and [2] indicate the theoretical values calculated in cases of both the high-spin and low-spin states of the Fe^{3+} ion; the line [1] is the high-spin state with the $(d\varepsilon)^3(d\gamma)^2$ configuration and the line [2] is the low-spin state with the $(d\varepsilon)^5(d\gamma)^0$ configuration.

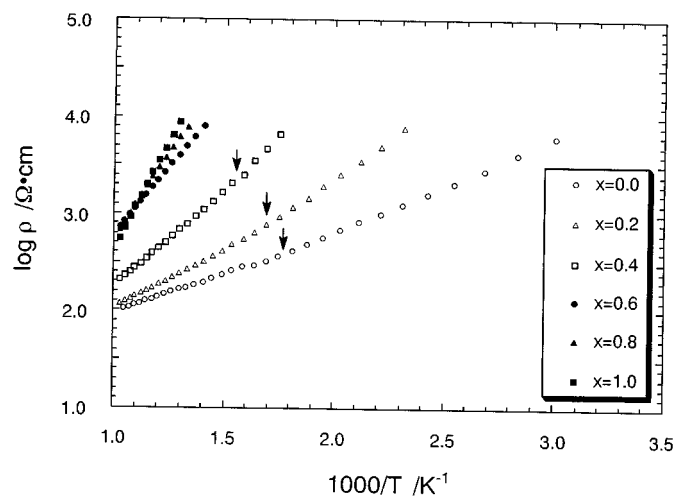

FIG. 4. Logarithm of the electrical resistivity (log ρ) vs $1000/T$ for the system $Nd(Cr_{1-x}Fe_x)O_3$. Arrow indicates the temperature (T_R) that the log ρ–$1000/T$ curve has the deflection.

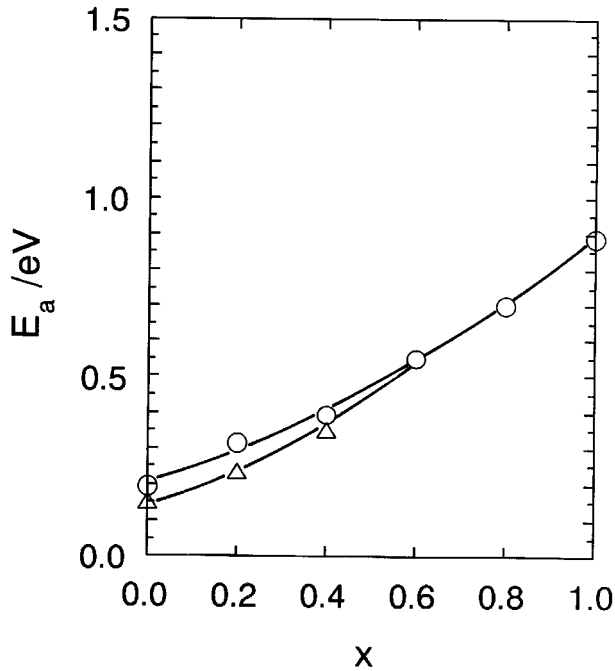

FIG. 5. Activation energy (E_a) vs composition (x) for the system $Nd(Cr_{1-x}Fe_x)O_3$. (○) E_a below T_R, (△) E_a above T_R.

are shown as the arrows in Fig. 4. The activation energy (E_a) calculated from the linear portion of $\log \rho$–$1000/T$ curves is shown in Fig. 5. In the range $0.0 \leq x \leq 0.4$, two values of E_a are shown by the calculation below T_R and above T_R. These values increase from ≈ 0.16 ($x = 0.0$) or ≈ 0.20 eV ($x = 0.0$) to ≈ 0.89 eV ($x = 1.0$). It is apparent that T_R is nearly equal to T_M.

Figure 6 shows the relationship between the Seebeck coefficient (α) and temperature. In the temperature range $500 \leq T \leq 1000$, α is positive and independent of temperature. Since the electrical resistivity of $NdFeO_3$ ($x = 1.0$) was very high, I could not obtain a reliable α below 780 K. At 800 K, α is $\approx 0.33 \pm 0.03$ mV/K for $0.0 \leq x \leq 0.6$, then decreases to ≈ 0.23 mV/K for $x = 0.8$ and ≈ 0.10 mV/K for $x = 1.0$. At T_R, the change in the α–T curves was not detected. In the case of a broad-band semiconductor, α is generally given by

$$\alpha = \pm \frac{k}{e}\left(\frac{E_F}{kT} + A\right), \tag{2}$$

where e is the electron charge, k is the Boltzmann constant, E_F is the Fermi energy, and A is a dimensionless constant depending on the details of the scattering mechanism (15). Equation (2) indicates that α shows a strong temperature dependence. However, the result in Fig. 6 is independent of temperature. For the explanation of the temperature independence of α, under the assumption that all other interaction effect are negligible, Tuller and Nowick proposed the equation

$$\alpha = \pm \frac{k}{e}\left\{\ln \beta\left(\frac{1-c}{c}\right) + \frac{S_T^*}{k}\right\} \tag{3}$$

for a hopping mechanism involving a fixed number of carriers (16). Here S_T^* is the vibration entropy and is small enough to be negligible. β is a degeneracy factor; for the case of $\beta = 1$, Eq. (3) is often referred to as the "Heikes formula" (16). c is the fraction of sites which contain an electron,

$$C = \frac{n}{N}, \tag{4}$$

where n is the number of electrons and N is the number of available sites per unit volume (V). By substituting Eq. (4)

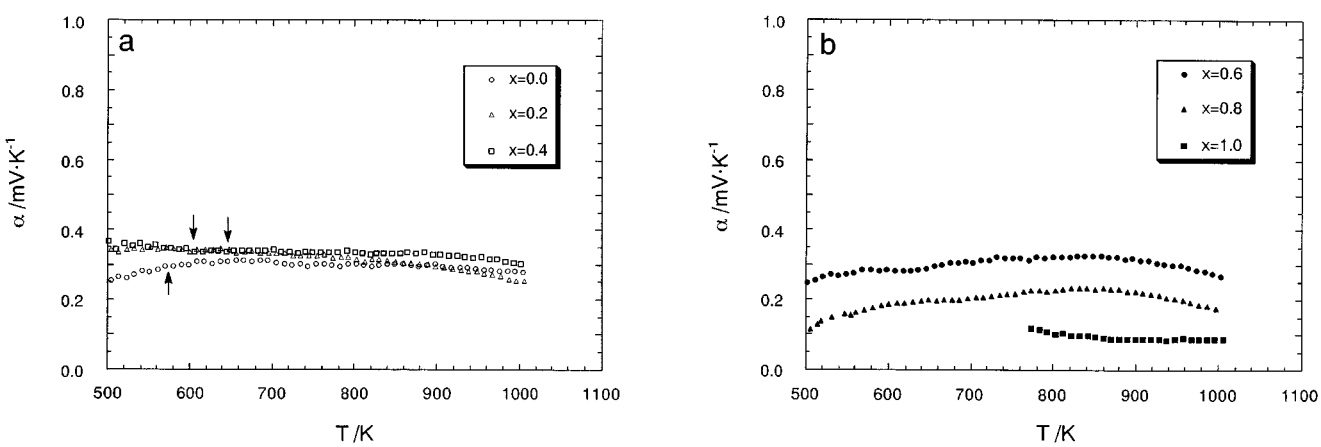

FIG. 6. Seebeck coefficient (α) vs temperature (T) for the system $Nd(Cr_{1-x}Fe_x)O_3$. Arrow indicates T_R.

into Eq. (3), n is easily calculated from α and N. The electrical conductivity (σ) is given by

$$\sigma = ne\mu, \tag{5}$$

where μ is the mobility. Since there are four sites in the orthorhombic perovskite-type unit cell, N is expressed as $N = 4/V$. The compositional increase of V at room temperature is small ($\approx 3.4\%$). Although V at 800 K was not measured, it is expected that V at 800 K is smaller than double V at room temperature and that the compositional increase of V at 800 K is also small. When the value of V at room temperature is used in the calculation, N is almost independent of x. From the variation of α, it is considered that n is independent of x in the range $0.0 \le x \le 0.6$ and increases with x in the range $0.8 \le x \le 1.0$. The electrical resistivity at 800 K is ≈ 157 for $x = 0.0$, ≈ 228 for $x = 0.2$, ≈ 592 for $x = 0.4$, ≈ 3300 for $x = 0.6$, ≈ 4560 for $x = 0.8$, and $\approx 7300\ \Omega \cdot$cm for $x = 1.0$, respectively. Consequently, μ decreases with x as follows; $\approx 8 \times 10^{-5}$ for $x = 0.0$, $\approx 6 \times 10^{-5}$ for $x = 0.2$, $\approx 3 \times 10^{-5}$ for $x = 0.4$, $\approx 7 \times 10^{-6}$ for $x = 0.6$, $\approx 1 \times 10^{-6}$ for $x = 0.8$, and $\approx 2 \times 10^{-7}\ cm^2 \cdot V^{-1} \cdot s^{-1}$ for $x = 1.0$, respectively.

Figure 7 shows DTA of $Nd(Cr_{1-x}Fe_x)O_3$ ($0.0 \le x \le 0.6$) in the temperature range $300 \le T \le 873$ K. Although TG showed no weight loss or weight in these samples, a broad and very weak exothermic peak was observed in the temperature $573 \le T \le 780$ K. The endothermic or exothermic peak due to the phase transition is usually sharp (17). Therefore, it is considered that the broad exothermic peak in Fig. 7 does not come from the phase transition, but the oxygen deficiency of the samples or the variation of the spin state of the Cr ion. However, the Cr^{3+} ion ($3d^3$) has only one electron configuration, $(d\varepsilon)^3(d\gamma)^0$. If there is a very small oxygen deficiency that is under the detection limits of TG,

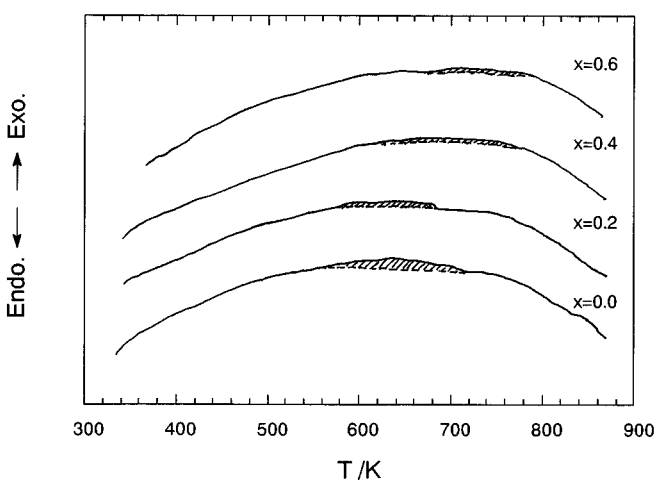

FIG. 7. DTA curves for the system $Nd(Cr_{1-x}Fe_x)O_3$.

a very small quantity of Cr^{2+} ions exist in the samples at high temperature. μ_{eff} calculated above T_M is larger than μ_{eff} calculated below T_M; μ_{eff} above T_M is $\approx 5.85\ \mu_B$ for $x = 0.0$, $\approx 5.92\ \mu_B$ for $x = 0.2$, and $\approx 5.91\ \mu_B$ for $x = 0.4$, respectively. It is obvious that the theoretical μ_{eff} with the high-spin state of the Cr^{2+} is larger than the theoretical μ_{eff} with the low-spin state of the Cr^{2+} ion. The increase of μ_{eff} above T_M is explained by the appearance of the small quantity of the Cr^{2+} ion. As seen in Fig. 5, E_a calculated above T_R is smaller than E_a calculated below T_R. It is obvious that the electrical resistivity is strongly influenced by the appearance of the Cr^{2+} ion.

Since the (Cr, Fe)O_6 octahedron in $Nd(Cr_{1-x}Fe_x)O_3$ connects with O(1) or O(2) of the neighboring (Cr, Fe)O_6 octahedron, there are two kinds of the cation–anion–cation overlap; one is an overlap (π-bonding) between the cation $d\varepsilon$ and oxygen p_π orbitals, and the other is the overlap (σ-bonding) between the cation $d\gamma$ and oxygen p_σ orbitals. According to Goodenough, three $3d$ electrons of the Cr^{3+} ion in $LaCrO_3$ are all localized and the Fermi level lies between the t_{2g}^* and narrow e_g^* levels (18). It is considered that $NdCrO_3$ has a same band structure as $LaCrO_3$ has; that is, both the localized t_{2g}^* and narrow e_g^* levels coexist and the intra-atomic exchange (Δ_{ex}) between the t_{2g}^*–α and t_{2g}^*–β levels is larger than the crystal-field splitting ($10Dq$) between the t_{2g}^* and e_g^* levels. With increasing x in $Nd(Cr_{1-x}Fe_x)O_3$, both the increase of the (Cr, Fe)–O distance and the decrease of the angles for (Cr, Fe)–O(1 and 2)–(Cr, Fe) make π-bonding decrease. Therefore, the cation–anion–cation overlap integrals (Δ_{cac}^{π} for π-bonding and Δ_{cac}^{σ} for σ-bonding) are smaller than the critical overlap integral (Δ_c); $\Delta_{cac}^{\pi} < \Delta_{cac}^{\sigma} < \Delta_c$ (19). Although the $3d$ electrons increases and exist in both the t_{2g}^* and e_g^* levels with increasing x, both the t_{2g}^* and e_g^* levels are localized and $10Dq$ increases, and so the mobility (μ) decreases and the electrical resistivity (ρ) increases as seen in Fig. 4. It is considered that a very small quantity of the Cr^{2+} ion forms other t_{2g}^* and e_g^* levels. $10Dq$ due to the Cr^{2+} ion is smaller than that due to the Cr^{3+} and Fe^{3+} ions, and the t_{2g}^* level of the Cr^{2+} ion is above the t_{2g}^* level of the Cr^{3+} and Fe^{3+} ions. Consequently, E_a becomes small above T_R as seen in Fig. 5.

CONCLUSION

The relationship between the crystal structure and the electrical properties of $Nd(Cr_{1-x}Fe_x)O_3$ was investigated from Rietveld analysis, the electrical resistivity, and Seebeck coefficient measurement. The increase of the (Cr, Fe)–O distance and μ_{eff} indicates that the Fe^{3+} ion in $Nd(Cr_{1-x}Fe_x)O_3$ is in the high-spin state with the $(d\varepsilon)^3(d\gamma)^2$ configuration. The $\log\rho$–$1000/T$ curves indicate that $Nd(Cr_{1-x}Fe_x)O_3$ is semiconductive with E_a of ≈ 0.16–≈ 0.89 eV. The Seebeck coefficient is almost independent of

temperature indicating that the mobility decreases with increasing x. The increase of the (Cr, Fe)–O distance and the decrease in the angles for (Cr, Fe)–O(1 and 2)–(Cr, Fe) make π-bonding decrease.

ACKNOWLEDGMENT

The author expresses his thanks to Dr. H. Kido, Osaka Municipal Technical Institute, for the magnetic measurements.

REFERENCES

1. T. Arakawa, S. Tsuchi-Ya, and J. Shiokawa, *Mater. Res. Bull.* **16,** 97 (1981).
2. J. B. Goodenough and J. M. Longo, *in* "Landolt–Bornstein, Numerical Data and Functional Relationships in Science and Technology. New Series, Group 3, Vol. 4, Magnetic and Other Properties of Oxides and Related Compounds" (K. H. Hellwege, Ed.), p. 228. Springer-Verlag, New York, 1971.
3. H. Taguchi, M. Nagao, and Y. Takeda, *J. Solid State Chem.* **114,** 236 (1995).
4. G. V. S. Rao, B. M. Wanklyn, and C. N. R. Rao, *J. Phys. Chem. Solids* **32,** 345 (1971).
5. R. D. Shannon, *Acta Crystallogr. Sect. A* **32,** 751 (1976).
6. W. Gordy, and J. O. Thomas, *J. Chem. Phys.* **24,** 439 (1956).
7. H. Taguchi, *J. Solid State Chem.* **118,** 367 (1995).
8. H. Taguchi, *J. Solid State Chem.* **122,** 297 (1996).
9. W. C. Koehler, E. O. Wollan, and M. K. Wilkinson, *Phys. Rev.* **118,** 58 (1960).
10. M. Eibschütz, G. Gorodetsky, S. Shtrikman, and D. Treves, *J. Appl. Phys.* **35,** 1071 (1964).
11. F. Izumi, *Nippon Kesho Gakkaishi* **27,** 23 (1985). [In Japanese]
12. R. D. Shannon, and C. T. Prewitt, *Acta Crystallogr. Sect. B* **25,** 925 (1969).
13. K. R. Poeppelmeier, M. E. Leonowicz, J. C. Scanlon, and W. B. Yelon, *J. Solid State Chem.* **45,** 71 (1982).
14. A. J. Dekker, "Solid State Physics," p. 450. Prentice–Hall, New York 1970.
15. J. H. Perlstein and M. J. Sienko, *J. Chem. Phys.* **48,** 174 (1968).
16. H. L. Tuller, and A. S. Nowick, *J. Phys. Chem. Solids* **38,** 859 (1977).
17. H. Taguchi, M. Nagao, T. Sato, and M. Shimada, *J. Solid State Chem.* **78,** 312 (1989).
18. J. B. Goodenough, *J. Appl. Phys.* **37,** 1415 (1966).
19. J. B. Goodenough, *Czech. J. Phys. B* **17,** 304 (1967).